

Dual-Prototype Disentanglement: A Context-Aware Enhancement Framework for Time Series Forecasting

Haonan Yang¹ Jianchao Tang¹ Zhuo Li¹

Abstract

Time series forecasting has witnessed significant progress with deep learning. While prevailing approaches enhance forecasting performance by modifying architectures or introducing novel enhancement strategies, they often fail to dynamically disentangle and leverage the complex, intertwined temporal patterns inherent in time series, thus resulting in the learning of static, averaged representations that lack context-aware capabilities. To address this, we propose the Dual-Prototype Adaptive Disentanglement framework (DPAD), a model-agnostic auxiliary method that equips forecasting models with the ability of pattern disentanglement and context-aware adaptation. Specifically, we construct a Dynamic Dual-Prototype bank (DDP), comprising a common pattern bank with strong temporal priors to capture prevailing trend or seasonal patterns, and a rare pattern bank dynamically memorizing critical yet infrequent events, and then an Dual-Path Context-aware routing (DPC) mechanism is proposed to enhance outputs with selectively retrieved context-specific pattern representations from the DDP. Additionally, we introduce a Disentanglement-Guided Loss (DGloss) to ensure that each prototype bank specializes in its designated role while maintaining comprehensive coverage. Comprehensive experiments demonstrate that DPAD consistently improves forecasting performance and reliability of state-of-the-art models across diverse real-world benchmarks.

1. Introduction

Time series forecasting (TSF) plays a pivotal role across numerous real-world domains, including weather forecasting

¹College of Computer Science and Technology, National University of Defense Technology, Changsha, China. Correspondence to: JianChao Tang <tangjianchao14@nudt.edu.cn>, Haonan Yang <yanghaonan21@nudt.edu.cn>.

(Bi et al., 2023; Wu et al., 2023b), transportation scheduling (Guo et al., 2020; Jin et al., 2021), healthcare monitoring (Tran et al., 2019; Wei et al., 2022), energy consumption (Alvarez et al., 2010; Guo et al., 2015) and finance (Chen et al., 2023; Yu et al., 2023). Due to the inherent non-stationarity and dynamics, traditional methods fail to effectively model intricate patterns across different time (Wang et al., 2024b; Chi et al., 2021). Recent advances in deep learning have demonstrated a strong capability for capturing intricate temporal dependencies in time series, making it a formidable tool for TSF (Wang et al., 2024a; Nie et al., 2023).

Prevailing research focuses on enhancing forecasting performance by modifying architectures (Wu et al., 2023a; 2021) or incorporating novel enhancement strategies (Kim et al., 2022; Liu et al., 2023), both of which have obviously improved the ability to model intricate nonlinear patterns (Qiu et al., 2024; Yang et al., 2025). To effectively capture complex temporal dependencies, some approaches have refined attention mechanisms (Liu et al., 2024a) or redesigned MLP and CNN architectures for improved modeling of long-range and cross-channel dependencies (Tang & Zhang, 2024; Luo & Wang, 2024). Meanwhile, some methods introduce enhancement strategies that directly encode prior knowledge about temporal structure into the learning process, which include explicit decomposition schemes that separate trend and seasonal components, as well as techniques such as post-processing to mitigate distribution shifts (Ning et al., 2025; Liu et al., 2025b).

Despite these advancements, TSF remains challenging due to the inherent complexity in real-world time series data (Wang et al., 2024c). This complexity stems primarily from the intrinsic non-stationarity and dynamics, leading to gradual or abrupt distribution shifts over time (Han et al., 2025). Consequently, the learned representations by models may suffer from temporal lag. Meanwhile, time series often exhibit intertwined and complex patterns(e.g., trends, seasonality, and irregular fluctuations) (Wang et al., 2025b), whose influences may vary across different periods and data (Hu et al., 2025). In these patterns, some critical yet rare patterns occur infrequently in historical observations, resulting in long-tail distributions that models often fail to adequately memorize (Liu et al., 2025b). These inherent

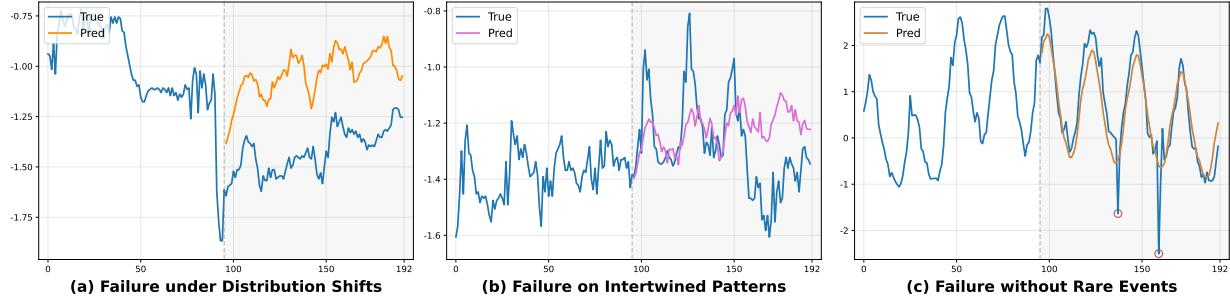


Figure 1. Limitation of static and averaged representations in time series forecasting. We visualize three characteristic failure scenarios where some methods fall short: (a) abrupt distribution shifts, (b) intertwined complex patterns, and (c) critical rare events. These limitations motivate our proposed context-aware enhancement framework.

challenges drive existing methods toward learning averaged, static representations, thereby hindering their ability to capture complex and context-sensitive temporal dependencies (Kudrat et al., 2025; Qiu et al., 2025b). To better illustrate this limitation, we select three representative real-world forecasting scenarios. As shown in Figure 1, a model relying on the static, average representations may struggle to adapt and disentangle individual patterns when confronted with distribution shifts and complex intertwined patterns. This phenomenon underscores the necessity of enhancing the model’s capability for dynamic disentanglement and adaptation to diverse temporal patterns.

To this end, we propose the Dual-Prototype Adaptive Disentanglement framework (DPAD), a novel, model-agnostic paradigm designed to overcome the limitation of static representations by endowing models with context-aware pattern disentanglement capabilities. Unlike prior works that modify the core architecture, DPAD functions as a plug-and-play auxiliary method that can be seamlessly integrated into various forecasting backbones. Specifically, our framework first establishes a learnable Dynamic Dual-Prototype bank (DDP), which comprises a common pattern bank covering prevalent and stable temporal modes, and a rare pattern bank dedicated to memorizing infrequent yet critical events. Then, a Dual-Path Context-aware routing (DPC) mechanism dynamically retrieves and activates relevant patterns from the DDP, thereby enhancing the backbone’s representation via a weighted gating strategy. Furthermore, our framework is optimized with a Disentanglement-Guided Loss (DGloss) that jointly ensures the separation of common and rare patterns, enforces diversity among common prototypes, and maintains the distinctiveness of rare prototypes. Our contributions are summarized as follows:

- We introduce a novel context-aware enhancement framework based on dual-prototype disentanglement. Unlike existing methods, our framework equips models with the capability for context-aware and pattern disentanglement, thereby directly mitigating the inher-

ent limitation of static representations and enhancing their ability to dynamically modeling intricate temporal patterns.

- We propose DPAD, a model-agnostic auxiliary framework that employs a learnable dual-prototype bank and an adaptive routing mechanism to dynamically enhance model’s prediction. A disentanglement-guided loss is further introduced to enforce effective pattern separation and preservation, which jointly optimizes the backbone and the prototype banks.
- Comprehensive experiments on multiple real-world datasets and state-of-the-art backbones demonstrate that DPAD consistently enhances forecasting performance with only negligible computational overhead.

2. Related Work

2.1. Time Series Forecasting Models

Recent years have witnessed remarkable progress in deep forecasting models, with their core advancement lying in learning more expressive temporal representations (Shao et al., 2025; Qiu et al., 2025a). Existing models can be broadly categorized by architecture into MLP-based, CNN-based, Transformer-based, and LLM-based approaches (Wang et al., 2024b). MLP-based architectures (Oreshkin et al., 2020; Tang & Zhang, 2024; Yi et al., 2023) often employ decomposition strategies and simple linear layers to capture cross-time dependencies, offering a compelling balance of efficiency and performance. CNN-based architectures (Bai et al., 2018; LIU et al., 2022; Wang et al., 2023) leverage hierarchical convolution structures and frequency-domain analysis (Wu et al., 2023a) to model local patterns and multi-periodicity effectively. Nevertheless, both of them often struggle to capture long-term dependencies. Therefore, Transformer-based architectures (Zhou et al., 2021; Chen et al., 2024; Liu et al., 2025a) have emerged as a powerful paradigm by introducing various efficient attention mechanisms to capture global dependencies. More

recently, LLM-based approaches (Liu et al., 2024b; Woo et al., 2024; Shi et al., 2025) have explored adapting pre-trained large language models for time series forecasting, leveraging their massive parameters and in-context learning capabilities. While excelling at capturing stable, recurring patterns, these models often tend to converge to a flexible representation (Zeng et al., 2023; Wang et al., 2025a). Consequently, they struggle to adaptively disentangle representations in response to the specific context of input sequences, such as distribution shifts, intricate mixtures of patterns, or the emergence of anomalies. This inherent rigidity underscores the need for a complementary mechanism that can inject contextual adaptability into these models.

2.2. Enhancement Strategies for Time Series Forecasting

Beyond architectural innovations, several efficient and model-agnostic strategies have been proposed to enhance predictive performance. Some methods employ decomposition strategies as a strong inductive bias to guide model in handling diverse temporal patterns more effectively (Huang et al., 2025; Wang et al., 2024a). Autoformer (Wu et al., 2021) decomposes time series into seasonal and trend components, allowing other models to handle input from a clearer perspective. TimesNet (Wu et al., 2023a) learns frequency-adaptive periods in the frequency domain to explicitly model intra- and inter-period variations. Another strategy focuses on model-agnostic methods (Liu et al., 2025c; Ning et al., 2025). RAFT (Han et al., 2025) employs retrieval augmented generation to retrieves from historical samples, providing the model with relevant information. HCAN (Sun et al., 2024) assigns class labels for timesteps to equip models with contextual-aware capability. Furthermore, specialized loss function designs have been designed to improve robustness against distribution shifts and intricate patterns (Wang et al., 2025a; Liu et al., 2025b). DBLoss (Qiu et al., 2025b) decomposes both predictions and ground truth to calculate the loss for each components separately. PSLoss (Kudrat et al., 2025) enhances structural alignment by comparing time series at the patch level with statistical properties. While these strategies improve forecasting performance, they still fail to dynamically disentangle complex, intertwined patterns in a context-aware manner. Different from them, our proposed DPAD framework introduces a learnable dual-prototype bank and adaptively fuses them through a context-aware routing mechanism, thereby enabling dynamic and interpretable enhancement of the backbone model’s representations with high efficiency.

3. Method

Time series forecasting addresses the fundamental challenge of predicting future values $Y = y_{t+1}, \dots, y_{t+h} \in \mathbb{R}^{h \times C}$

from historical observations $X = x_1, \dots, x_t \in \mathbb{R}^{t \times C}$, where h is the prediction horizon, t is the history horizon, and C is the number of variables.

3.1. Structure Overview

As illustrated in Figure 2, our proposed DPAD consists of three key components: (a) Dynamic Dual-Prototype Bank (DDP) that maintains a set of common and rare pattern prototypes to explicitly disentangle different patterns and dynamically update; (b) Dual-Path Context-aware routing (DPC) that dynamically retrieves and activates relevant prototypes from DDP, in which the representation is generated by an arbitrary backbone model, and then enhances the prediction through a weighted gating strategy; (c) Disentanglement-Guided Loss (DGloss) that jointly optimizes DDP and the backbone model through a quadruple loss formulation, which ensures both the specialization and separation of the prototypes.

3.2. Dynamic Dual-Prototype Bank

The Dynamic Dual-Prototype bank (DDP) serves as the cornerstone of our framework, designed to explicitly disentangle and memorize two distinct categories of temporal patterns: prevalent common patterns and critical yet infrequent rare patterns. Formally, the DDP consists of two separate prototype sets: a Common Pattern Bank \mathcal{B}_c , which comprise sequences synthesized from a combination of fundamental trends and seasonal patterns, and a Rare Pattern Bank \mathcal{B}_r , dedicated to memorizing long-tailed, sudden events and some other temporal noise.

Specifically, we generate two groups of base sequences $\{\mathbf{s}_c^i\}$ and rare sequences $\{\mathbf{s}_r^j\}$ using distinct prior strategies to reflect their different pattern characteristics:

$$\mathbf{s}_c^i \sim \mathcal{GP}(0, \lambda_l K_l + \lambda_r K_r + \lambda_p K_p), \quad i = 1, \dots, M, \quad (1)$$

$$\mathbf{s}_r^j \sim \mathcal{N}(0, \sigma^2 \mathbf{I}), \quad j = 1, \dots, N, \quad (2)$$

where \mathbf{s}_c^i denotes the common sequences generated via a mixture of Gaussian Process \mathcal{GP} kernels to embed strong temporal priors, and K_l, K_r, K_p are the Linear, radial basis function (RBF), and Periodic kernel, λ_i is mixing coefficients. This strategy yields diverse yet structured prototypes that cover stable, recurring patterns such as trends, seasonality, and their mixtures, thereby providing a well-initialized basis for modeling prevalent temporal dynamics.

In contrast, \mathbf{s}_r^j is initialized from Gaussian distribution $\mathcal{N}(0, \sigma^2 \mathbf{I})$, where σ^2 is a small variance controlling the magnitude of initialization noise. This minimal random initialization ensures that rare prototypes begin from an nearly unbiased state, allowing them to remain flexible and exclusively adapt to capture rare patterns during training, without

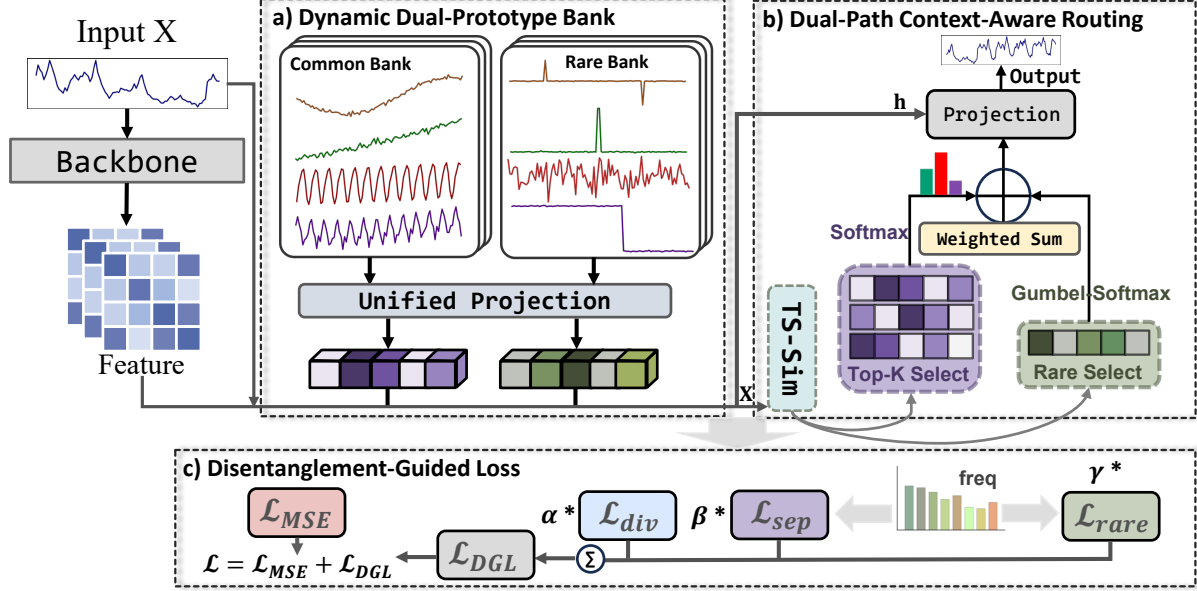


Figure 2. The overall architecture of the DPAD framework. The framework constructs a learnable dual-prototype bank, then performs adaptive dual-path routing on the input data to retrieve relevant prototypes, and finally generates a context-aware enhancement for prediction. The entire framework is optimized under a disentanglement-guided loss.

being predisposed to common modes. Notably, all of sequence sets would be transformed into learnable parameters.

Then each generated sequence is projected into a shared D -dimensional latent space via the linear layers:

$$\mathbf{p}_c^i = \mathbf{Proj}_c(\mathbf{s}_c^i), \quad (3)$$

$$\mathbf{p}_r^j = \mathbf{Proj}_r(\mathbf{s}_r^j), \quad (4)$$

The resulting Common Pattern Bank \mathcal{B}_c and Rare Pattern Bank \mathcal{B}_r are defined as follows:

$$\mathcal{B}_c = \{\mathbf{p}_c^1, \mathbf{p}_c^2, \dots, \mathbf{p}_c^M\}, \quad \mathcal{B}_r = \{\mathbf{p}_r^1, \mathbf{p}_r^2, \dots, \mathbf{p}_r^N\}, \quad (5)$$

This strategy explicitly separates the modeling of common and rare patterns while keeping the prototype representation compact and adaptive. Both \mathcal{B}_c and \mathcal{B}_r are updated throughout training under the guidance of the disentanglement loss described in Section 3.4. This allows the common prototypes to evolve toward more representative and dataset-specific stable patterns, while the rare prototypes dynamically adapt to capture and memorize infrequent yet critical temporal patterns.

3.3. Dual-Path Context-Aware Routing

Dual-Path Context-aware routing (DPC) mechanism is proposed to adaptively enhance final prediction. Given the input \mathbf{X} and its contextual representation $\mathbf{h} \in \mathbb{R}^D$ from the backbone model, and our DPC dynamically retrieves and fuses relevant patterns from the DDP through a dual-path

design. Specifically, we first compute the similarity scores ρ_c and ρ_r between the input \mathbf{X} and each prototype in \mathcal{B}_c and \mathcal{B}_r :

$$\rho_c = s(\mathbf{X}, \mathcal{B}_c), \quad \rho_r = s(\mathbf{X}, \mathcal{B}_r), \quad (6)$$

Here we adopt the Pearson Correlation as the similarity measurement $s(\cdot, \cdot)$, which provides scale-invariant matching that focuses on the shape similarity of temporal patterns. We then employ a dual-path selection strategy to retrieve the most relevant prototypes:

$$\mathcal{I}_c = \arg \text{top-K}(\rho_i | 1 \leq i \leq K), \quad (7)$$

$$\mathcal{I}_r = \begin{cases} \arg \max(\rho_r), & \text{if } \max(\rho_r) > \epsilon \\ \emptyset, & \text{otherwise} \end{cases} \quad (8)$$

For the common bank \mathcal{B}_c , we select top-K prototypes with the highest similarity scores, forming an index set \mathcal{I}_c . Conversely, to enforce sparsity and precise memory for rare events, we select at most one prototype from the rare bank \mathcal{B}_r , with its index denoted as \mathcal{I}_r .

Then we compute adaptive weights for the selected common prototypes:

$$\omega_c = \text{Softmax}(\rho_c[\mathcal{I}_c]/\tau), \quad (9)$$

For the rare path, a sparse weight vector \mathcal{B}_r is generated by one-hot activation. The retrieved pattern contributions are then computed as weighted sums:

$$\mathbf{z}_c = \sum_{k \in \mathcal{I}_c} \omega_c^k \cdot \mathcal{B}_c[k], \quad \mathbf{z}_r = \omega_r \cdot \mathcal{B}_r[\mathcal{I}_r], \quad (10)$$

Finally, these context-aware contributions are fused with the backbone representation \mathbf{h} through concatenation and a linear projection to produce the enhanced prediction \mathbf{Y} :

$$\mathbf{Y} = \mathbf{W}_o[\mathbf{h}; \mathbf{z}_c; \mathbf{z}_r], \quad (11)$$

This adaptive fusion mechanism thereby enhances the capability of the model to dynamically disentangle intricate temporal dependencies, which mitigates the inherent limitation of static, averaged representations.

3.4. Disentanglement-Guided Loss

To ensure the DDP learns a well-disentangled and effective representation of common and rare patterns, we propose a Disentanglement-Guided Loss (DGloss). This loss function jointly optimizes the parameters of backbone model and the DDP by enforcing three key properties: pattern separation, rarity preservation, and common set diversity.

We first introduce the Separation Loss \mathcal{L}_{sep} to ensure a clear functional divide between the common and rare banks, preventing role confusion. Guided by pattern frequency statistics within a training batch, \mathcal{L}_{sep} dynamically encourages each bank to specialize in its respective domain:

$$\mathcal{L}_{\text{sep}} = \mathbb{E}[\omega \cdot \max(0, m - \Delta\rho) + (1 - \omega) \cdot \max(0, m + \Delta\rho)], \quad (12)$$

where $\Delta\rho$ is the difference between similarities ρ_c and ρ_r , m is a margin, and $\omega \in [0, 1]$ is a frequency weight. Intuitively, if the input contains patterns frequently observed in recent batches, the loss penalizes activation of the rare bank; conversely, for a rare input pattern, it penalizes over-reliance on the common bank.

Then we propose a Rarity Preservation Loss $\mathcal{L}_{\text{rare}}$. With the contrastive restriction, $\mathcal{L}_{\text{rare}}$ prevent the prototypes in the rare bank from being contaminated or forgotten due to common patterns, thereby ensuring their persistent memory for rare patterns:

$$\mathcal{L}_{\text{rare}} = -\frac{1}{|\mathcal{A}|} \sum_{k \in \mathcal{A}} \log \left[\frac{\exp(\frac{s_{kk}}{\tau})}{\sum_{j=1}^N \exp(\frac{s_{kj}}{\tau})} \right], \quad (13)$$

where \mathcal{A} is the set of activated rare prototype indices for the input, s_{kj} denotes the similarity between the input representation and the j -th rare prototype. $\mathcal{L}_{\text{rare}}$ pulls the input representation closer to the activated rare prototype in the latent space while pushing it away from other rare prototypes.

Furthermore, we adopt a diversity loss \mathcal{L}_{div} that leverages orthogonal constraints to promote diversity and reduce redundancy among common prototypes, thereby ensuring the common bank covers a more comprehensive range of prevalent patterns:

$$\mathcal{L}_{\text{div}} = \frac{1}{M(M-1)} \sum_{i=1}^M \sum_{j \neq i}^M \left(\frac{\mathbf{p}_c^i \top \mathbf{p}_c^j}{\|\mathbf{p}_c^i\| \|\mathbf{p}_c^j\|} \right)^2, \quad (14)$$

where M is the number of common prototypes and \mathbf{p}_c^i is the i -th common prototype vector.

Finally, we integrated this three loss terms as the Disentanglement - Guided Loss \mathcal{L}_{DGL} :

$$\mathcal{L}_{\text{DGL}} = \lambda_{\text{sep}} \mathcal{L}_{\text{sep}} + \lambda_{\text{rare}} \mathcal{L}_{\text{rare}} + \lambda_{\text{div}} \mathcal{L}_{\text{div}}, \quad (15)$$

where λ_{sep} , λ_{rare} , λ_{div} are balancing coefficients. The total loss function is formulated as follows:

$$\mathcal{L} = \mathcal{L}_{\text{MSE}} + \mathcal{L}_{\text{DGL}} \quad (16)$$

By explicitly coordinating the separation, preservation, and diversity of temporal prototypes, our DGloss shapes a well-structured and disentangled pattern memory. This mechanism enables the model to dynamically retrieve context-aware patterns, effectively mitigating the limitation of static representation.

4. Experiments

To comprehensively verify the performance and effectiveness of the proposed DPAD, we conduct extensive experiments on both long-term and short-term forecasting tasks.

4.1. Experimental Setup

Datasets. For long-term forecasting, we conduct experiments on six well-known benchmarks, including ETT (ETTh1, ETTh2, ETTm1, ETTm2), Electricity, Exchange, Solar, Weather, and Traffic. Meanwhile, we utilize PEMS (PEMS03, PEMS04, PEMS07, PEMS08) for short-term forecasting. Detailed information about the datasets is provided in the Section A.

Baselines. To verify the performance and effectiveness of our DPAD, we select five state-of-art (SOTA) time series forecasting models with diverse architectures, including transformer-based models: iTransformer (Liu et al., 2024a), TimeXer (Wang et al., 2024c), TimeBridge (Liu et al., 2025a); MLP-based models: DLinear (Zeng et al., 2023); and CNN-based models: TimesNet (Wu et al., 2023a).

Implementation Details. All experiments are implemented in Pytorch, and conducted on a single NVIDIA RTX 4090 24 GB GPU. We utilize ADAM optimizer with an initial learning rate 10^{-3} and L2 loss for model optimization. For fair evaluation, we use the framework of TimesNet (Wu et al., 2023a), and all the baselines are implemented based on the configurations of original paper and its code.

4.2. Main Results

We present the main results for both long-term and short-term forecasting on seven real-world datasets for five state-of-art forecasting models in Table 1, where the lower MSE

Table 1. Forecasting results for long-term and short-term. The look-back length is fixed to 96 for all baselines. All the results are averaged from 4 different prediction lengths, that is $\{12, 24, 48, 96\}$ for PEMS and $\{96, 192, 336, 720\}$ for others. The better results are highlighted in **bold**. See Section E.1 for full results.

Methods		iTransformer	+ DPAD	DLinear	+ DPAD	TimesNet	+ DPAD	TimeXer	+ DPAD	TimeBridge	+ DPAD
ETTh1	MSE	0.452	0.446	0.461	0.449	0.479	0.476	0.460	0.442	0.450	0.432
	MAE	0.446	0.439	0.457	0.450	0.466	0.463	0.452	0.441	0.443	0.431
ETTh2	MSE	0.383	0.376	0.563	0.529	0.411	0.396	0.373	0.369	0.379	0.367
	MAE	0.406	0.399	0.518	0.500	0.420	0.414	0.403	0.396	0.403	0.391
ETTm1	MSE	0.407	0.401	0.404	0.394	0.418	0.400	0.390	0.386	0.387	0.379
	MAE	0.412	0.405	0.407	0.404	0.417	0.409	0.395	0.394	0.399	0.387
ETTm2	MSE	0.292	0.285	0.354	0.334	0.291	0.281	0.277	0.299	0.281	0.282
	MAE	0.335	0.329	0.402	0.391	0.330	0.325	0.322	0.318	0.326	0.321
Electricity	MSE	0.175	0.170	0.225	0.214	0.193	0.196	0.201	0.170	0.171	0.165
	MAE	0.264	0.261	0.319	0.305	0.293	0.296	0.275	0.268	0.266	0.256
Exchange	MSE	0.361	0.354	0.338	0.345	0.201	0.384	0.398	0.375	0.417	0.361
	MAE	0.406	0.401	0.413	0.417	0.446	0.422	0.422	0.409	0.440	0.402
Solar	MSE	0.237	0.233	0.330	0.264	0.267	0.244	0.226	0.220	0.236	0.231
	MAE	0.264	0.256	0.401	0.308	0.286	0.276	0.269	0.262	0.270	0.241
Traffic	MSE	0.422	0.416	0.688	0.613	0.633	0.511	0.466	0.463	0.912	0.444
	MAE	0.282	0.278	0.427	0.385	0.333	0.318	0.286	0.284	0.544	0.286
Weather	MSE	0.260	0.256	0.265	0.259	0.256	0.244	0.242	0.239	0.258	0.256
	MAE	0.281	0.276	0.316	0.317	0.283	0.272	0.272	0.270	0.281	0.273
PEMS03	MSE	0.260	0.188	0.279	0.197	0.153	0.125	0.180	0.134	0.153	0.155
	MAE	0.327	0.283	0.377	0.301	0.254	0.229	0.279	0.248	0.262	0.259
PEMS04	MSE	0.912	0.199	0.295	0.205	0.138	0.111	0.326	0.138	0.193	0.192
	MAE	0.801	0.312	0.388	0.313	0.250	0.222	0.418	0.261	0.295	0.289
PEMS07	MSE	0.109	0.104	0.328	0.223	0.109	0.105	0.088	0.089	0.128	0.130
	MAE	0.214	0.207	0.394	0.310	0.216	0.206	0.192	0.192	0.232	0.230
PEMS08	MSE	0.199	0.173	0.403	0.272	0.198	0.160	0.205	0.179	0.168	0.164
	MAE	0.278	0.254	0.444	0.323	0.236	0.235	0.248	0.262	0.255	0.251

and MAE indicate better forecasting performance. Our proposed DPAD framework demonstrates consistent improvements across all backbone models, achieving the lowest MSE and MAE in most cases. Notably, DPAD achieves an average MSE reduction of 12.6% for DLinear and 9.3% for iTransformer, and follows a similar trend for other backbones. The performance gains are particularly substantial on datasets with inherent complexities such as Traffic and PEMS. These reduction demonstrates the effectiveness of our model-agnostic design, which equips diverse architectures with context-aware and pattern disentanglement capability without modifying their core structure. The above observations highlight the efficacy of DPAD in mitigating the inherent limitations of static representation in forecasting models.

4.3. Ablation Studies

To validate the contribution of each component in our DPAD framework, systematic ablation experiments were conducted on Electricity, Weather, Traffic and Solar datasets. The results are presented in Table 2, Table 3, and Table 4, which correspond to the ablations of the DDP, DPC, and DGloss

modules, respectively.

For the Dynamic Dual-Prototype bank (DDP) components, we performed the following experiments: ① without the complete DDP, ② with only the Common Bank, ③ with only the Rare Bank. As shown in Table 2, the significant performance degradation observed upon removing the entire DDP confirms its overall effectiveness. Moreover, ablating either prototype bank individually impairs forecasting performance. This demonstrates the benefit of explicitly maintaining separate representations for common and rare patterns, which is especially critical in real-world datasets characterized by complex, intertwined patterns.

For the Dual-Path Context-aware routing (DPC) mechanism, we evaluated two alternative fusion strategies: ① adopts element-wise sum fusion, replacing adaptive retrieval with a simple summation of prototype vectors, and ② employs fixed average fusion, substituting it with static average weighting. The results in Table 3 show that both fixed fusion strategies underperform our adaptive routing mechanism. This indicates that static fusion lacks dynamic selection and weighting mechanisms based on input context, thereby weakening the enhancement effect. It highlights the core

Table 2. Ablation study on DDP to validate the efficacy of Common Pattern Bank and Rare Pattern Bank. ✓ and ✗ indicate with and without certain components respectively. All the results are averaged from 4 different prediction lengths {96, 192, 336, 720}, see Section E.2 for full results.

Case	Common		Rare		Electricity		Weather		Traffic		Solar	
	Bank	Bank	MSE	MAE	MSE	MAE	MSE	MAE	MSE	MAE	MSE	MAE
①	✗	✗	0.175	0.264	0.260	0.281	0.422	0.282	0.237	0.262		
②	✓	✗	0.178	0.269	0.262	0.282	0.362	0.314	0.240	0.266		
③	✗	✓	0.183	0.272	0.263	0.282	0.423	0.283	0.237	0.262		
④	✓	✓	0.170	0.261	0.256	0.276	0.416	0.278	0.233	0.256		

functionality of our DPC mechanism, which dynamically adjusts the contribution of retrieved prototypes according to specific input contexts.

Table 3. Ablation study on DPC to compare adaptive routing with different static fusion strategies.

Case	Electricity		Weather		Traffic		Solar	
	MSE	MAE	MSE	MAE	MSE	MAE	MSE	MAE
① w/ Additive	0.179	0.268	0.262	0.282	0.422	0.282	0.237	0.268
② w/ Mean	0.177	0.269	0.260	0.281	0.439	0.298	0.237	0.262
③ Full DPC	0.170	0.261	0.256	0.276	0.416	0.278	0.233	0.256

For the Disentanglement-Guided Loss (DGloss), we conduct experiments as follows: ① removes all components in DGloss, ② removes the separation loss \mathcal{L}_{sep} , ③ removes the rarity preservation loss \mathcal{L}_{rare} , and ④ removes the diversity loss \mathcal{L}_{div} . As shown in Table 4, removing any individual loss term or the whole DGloss leads to a performance drop. Training without these specialized constraints fails to effectively optimize the interaction between the model and our prototype banks. Meanwhile, without explicit guidance for separation, diversity, and rarity preservation, our DDP cannot learn a well-disentangled representation, and their synergistic effect will be severely compromised. Therefore, DGloss serves as a core component that ensures effective pattern disentanglement and stable prototype memory formation.

Table 4. Ablation study on DGloss to assess the contribution of each loss component.

Case	\mathcal{L}_{sep}			\mathcal{L}_{div}			Electricity		Weather		Traffic		Solar	
	MSE	MAE	\mathcal{L}_{sep}	MSE	MAE	\mathcal{L}_{div}	MSE	MAE	MSE	MAE	MSE	MAE	MSE	MAE
①	✗	✗	✗	0.180	0.271	0.264	0.283	0.441	0.298	0.241	0.267			
②	✗	✓	✓	0.178	0.269	0.262	0.281	0.464	0.322	0.239	0.266			
③	✓	✗	✓	0.179	0.268	0.261	0.282	0.450	0.308	0.239	0.266			
④	✓	✓	✗	0.177	0.269	0.262	0.283	0.441	0.299	0.238	0.265			
⑤	✓	✓	✓	0.170	0.261	0.256	0.276	0.416	0.278	0.233	0.256			

4.4. Zero-Shot Forecasting

To further evaluate the generalization and robustness of our DPAD on unseen datasets, we conduct zero-shot forecasting experiments. Following by prior works(Kudrat et al.,

2025; Jin et al., 2024), we sequentially use ETTh1, ETTh2, ETTm1, and ETTm2 as source datasets, and the remaining datasets as target datasets.

Table 5 shows zero-shot results with four backbone models, which consistently demonstrate that models enhanced with our DPAD framework achieve superior performance in most cases. These improvements indicate that the disentangled pattern memory in DPAD provides a more transferable and robust temporal representation. Specifically, the common prototypes in DDP learn domain-invariant, prevalent patterns that serve as reusable components across different datasets. Meanwhile, the DPC mechanism enables the model to dynamically integrate these prototypes, and activate sparse rare prototypes when necessary, which could account for novel, target-specific variations without requiring retraining. Consequently, these zero-shot results underscore that DPAD not only enhances forecasting performance for in-distribution data, but learns temporal patterns with more generalization.

4.5. Model Analysis

Prototype Visualization. To provide an intuitive understanding of what the DDP learns, we visualize the temporal forms of several representative prototypes from both the common and rare bank on the Weather dataset. As shown in Figure 3, the prototypes in both the common bank and rare bank evolve dynamically during training. For the common bank, the learned prototypes consistently exhibit smooth, structured shapes, including stable hybrid patterns that combine trend and seasonality components. These patterns correspond well to the intricate dependencies of the dataset, confirming that our initialization provides effective guidance and that the common bank successfully captures and refines these prevalent patterns through training. In contrast, the rare bank displays markedly different characteristics, whose prototypes are characterized by abrupt, irregular fluctuations or sudden shifts. These patterns do not conform to regular seasonal or trend patterns, which demonstrates the capability of rare set to memorize infrequent yet critical events as well as some other fluctuations.

Increasing Look-Back Length. A longer look-back sequence provides richer historical information in principle, yet also presents a greater challenge due to the more complex temporal dependencies it includes. To evaluate the capability of DPAD to disentangle and leverage long-range historical context, we conduct experiments under increasing look-back length {48, 96, 192, 336, 720} on the Electricity dataset, taking TimeBridge as backbone model. As shown in Figure 4, DPAD consistently achieves greater performance gains over the backbone as the sequence length increases. While vanilla backbones may suffer from information overload or struggle to focus on long-term dependencies, DPAD

Table 5. Zero-shot forecasting results on ETT datasets. The forecasting length is set to 96. And the better results are highlighted in **bold**.

Methods		iTransformer		+DPAD		DLinear		+DPAD		TimesNet		+DPAD		TimeXer		+DPAD	
Source	Target	MSE	MAE														
ETTh1	ETTh2	0.419	0.428	0.416	0.425	0.495	0.487	0.489	0.481	0.480	0.459	0.439	0.443	0.426	0.429	0.420	0.425
	ETTm1	0.822	0.585	0.834	0.596	0.749	0.579	0.746	0.576	0.849	0.575	0.754	0.571	0.832	0.591	0.798	0.575
	ETTm2	0.342	0.375	0.339	0.373	0.409	0.454	0.405	0.451	0.368	0.390	0.339	0.370	0.344	0.374	0.341	0.370
ETTh2	ETTh1	0.694	0.581	0.632	0.547	0.544	0.508	0.539	0.504	0.802	0.623	0.769	0.602	0.695	0.577	0.666	0.558
	ETTm1	0.980	0.631	0.904	0.606	0.768	0.594	0.783	0.605	1.059	0.658	1.043	0.644	1.428	0.748	1.412	0.734
	ETTm2	0.358	0.389	0.346	0.378	0.537	0.541	0.526	0.532	0.369	0.394	0.380	0.404	0.387	0.408	0.377	0.402
ETTm1	ETTh1	0.718	0.571	0.670	0.549	0.614	0.530	0.602	0.522	0.952	0.694	0.930	0.660	0.960	0.662	0.948	0.643
	ETTh2	0.482	0.465	0.476	0.459	0.500	0.492	0.492	0.479	0.566	0.515	0.555	0.507	0.591	0.522	0.578	0.507
	ETTm2	0.326	0.362	0.312	0.351	0.318	0.356	0.337	0.367	0.357	0.380	0.340	0.369	0.336	0.364	0.341	0.371
ETTm2	ETTh1	1.214	0.748	0.980	0.676	0.634	0.554	0.611	0.523	0.993	0.655	0.872	0.619	0.734	0.578	0.709	0.576
	ETTh2	0.553	0.507	0.519	0.487	0.508	0.499	0.519	0.506	0.528	0.487	0.490	0.472	0.457	0.453	0.436	0.425
	ETTm1	0.825	0.589	0.804	0.579	0.561	0.498	0.544	0.479	0.709	0.554	0.701	0.548	0.647	0.531	0.631	0.525

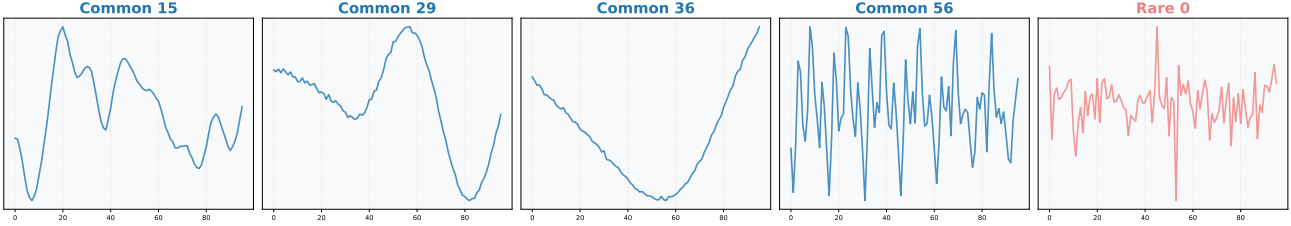


Figure 3. Visualization of learned prototypes in DDP on the Electricity dataset.

helps them utilize the extended history information more effectively. These results indicate that components in DPAD are particularly effective at capturing, disentangling, and selectively leveraging relevant intertwined patterns from long sequences. Our framework provides a structured mechanism to deal with the expanded context.

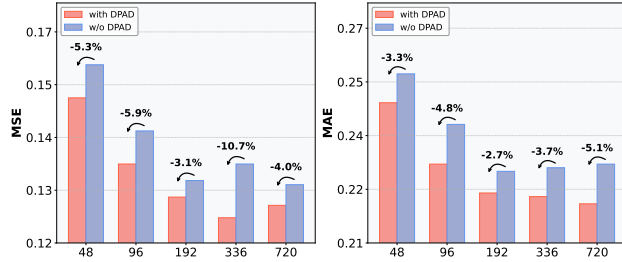


Figure 4. Forecasting results (MSE and MAE) with varying look-back length {48, 96, 192, 336, 720} on Electricity dataset. Prediction length is fixed to 96.

Efficiency Analysis. We conduct the efficiency analysis for the backbone model with and without DPAD. As shown in Table 6, DPAD introduces minimal overhead for most backbone models. The relative increases in running time and memory footprint are generally modest, which is below 10% for most Transformer or CNN-based backbones. While a lightweight model like DLinear shows a higher relative increase due to its extremely small base cost, the absolute added overhead remains minimal. This demonstrates DPAD is a practical and efficient enhancement module, delivering

significant performance improvements while incurring only a small fraction of additional computational cost.

Table 6. Comparison of efficiency analysis for backbone models with and without DPAD. The results are recorded on the Electricity dataset with batch size is set to 16. The look-back length and prediction length is fixed to 96. Running time means running time per iteration. $\Delta\%$ denotes the relative change rate.

Metrics	Running Time			Memory Footprint		
	Methods	ori	+DPAD	$\Delta\%$	ori	+DPAD
iTransformer	17ms	20ms	17.6%	782MB	820MB	4.8%
TimeXer	119ms	126ms	5.8%	4634MB	4746MB	2.4%
TimeBridge	98ms	107ms	9.1%	4240MB	4334MB	2.2%
DLinear	7ms	11ms	57.1%	62MB	90MB	45.1%
TimesNet	262ms	266ms	1.5%	3332MB	3470MB	4.1%

5. Conclusion

In this paper, we address a critical limitation of static and averaged representations in deep time series forecasting, which hinders model adaptability to intricate and dynamic contexts. We propose the Dual-Prototype Adaptive Disentanglement (DPAD) framework, a model-agnostic auxiliary method that enhances backbone model through a Dynamic Dual-Prototype bank (DDP), Dual-Path Context-aware routing (DPC), and a Disentanglement-Guided Loss (DGloss). Extensive experiments validate that DPAD consistently improves forecasting performance while introduces minimal computational overhead. Future work may explore more interpretable routing mechanisms and novel prototype paradigm with multi-modal representations.

References

Alvarez, F. M., Troncoso, A., Riquelme, J. C., and Ruiz, J. S. A. Energy time series forecasting based on pattern sequence similarity. *IEEE Transactions on Knowledge and Data Engineering*, 23(8):1230–1243, 2010.

Bai, S., Kolter, J. Z., and Koltun, V. An empirical evaluation of generic convolutional and recurrent networks for sequence modeling, 2018.

Bi, K., Xie, L., Zhang, H., Chen, X., and Gu, X. Accurate medium-range global weather forecasting with 3d neural networks. *Nature*, 619(7970):533–538, 2023.

Chen, P., Zhang, Y., Cheng, Y., Shu, Y., Wang, Y., Wen, Q., Yang, B., and Guo, C. Pathformer: Multi-scale transformers with adaptive pathways for time series forecasting. In *12th International Conference on Learning Representations, ICLR 2024*, 2024.

Chen, Z., Zheng, L., Lu, C., Yuan, J., and Zhu, D. Chatgpt informed graph neural network for stock movement prediction. *SSRN Electronic Journal*, 2023. ISSN 1556-5068.

Chi, H., Liu, F., Yang, W., Lan, L., Liu, T., Han, B., Cheung, W., and Kwok, J. Tohan: A one-step approach towards few-shot hypothesis adaptation. *Advances in neural information processing systems*, 34:20970–20982, 2021.

Guo, C., Yang, B., Andersen, O., Jensen, C. S., and Torp, K. Ecomark 2.0: empowering eco-routing with vehicular environmental models and actual vehicle fuel consumption data. *GeoInformatica*, 19(3):567–599, 2015.

Guo, C., Yang, B., Hu, J., Jensen, C. S., and Chen, L. Context-aware, preference-based vehicle routing. *The VLDB Journal*, 29(5):1149–1170, 2020.

Han, S., Lee, S., Cha, M., Arik, S. O., and Yoon, J. Retrieval augmented time series forecasting, 2025.

Hu, Y., Liu, P., Zhu, P., Cheng, D., and Dai, T. Adaptive multi-scale decomposition framework for time series forecasting, 2025.

Huang, S., Zhao, Z., Li, C., and Bai, L. Timekan: Kan-based frequency decomposition learning architecture for long-term time series forecasting, 2025.

Jin, K., Wi, J., Lee, E., Kang, S., Kim, S., and Kim, Y. Trafficbert: Pre-trained model with large-scale data for long-range traffic flow forecasting. *Expert Systems with Applications*, 186:115738, 2021.

Jin, M., Wang, S., Ma, L., Chu, Z., Zhang, J. Y., Shi, X., Chen, P.-Y., Liang, Y., Li, Y.-F., Pan, S., and Wen, Q. Time-llm: Time series forecasting by reprogramming large language models, 2024.

Kim, T., Kim, J., Tae, Y., Park, C., Choi, J.-H., and Choo, J. Reversible instance normalization for accurate time-series forecasting against distribution shift. In *10th International Conference on Learning Representations, ICLR 2022*, 2022.

Kudrat, D., Xie, Z., Sun, Y., Jia, T., and Hu, Q. Patch-wise structural loss for time series forecasting, 2025.

LIU, M., Zeng, A., Chen, M., Xu, Z., LAI, Q., Ma, L., and Xu, Q. Scinet: Time series modeling and forecasting with sample convolution and interaction. In *Advances in Neural Information Processing Systems*, volume 35, pp. 5816–5828, 2022.

Liu, P., Wu, B., Hu, Y., Li, N., Dai, T., Bao, J., and tao Xia, S. Timebridge: Non-stationarity matters for long-term time series forecasting, 2025a.

Liu, Y., Hu, T., Zhang, H., Wu, H., Wang, S., Ma, L., and Long, M. itransformer: Inverted transformers are effective for time series forecasting, 2024a.

Liu, Y., Zhang, H., Li, C., Huang, X., Wang, J., and Long, M. Timer: Generative pre-trained transformers are large time series models. In *41st International Conference on Machine Learning, ICML 2024*, 2024b.

Liu, Z., Cheng, M., Li, Z., Huang, Z., Liu, Q., Xie, Y., and Chen, E. Adaptive normalization for non-stationary time series forecasting: A temporal slice perspective. In *37th Conference on Neural Information Processing Systems, NeurIPS 2023*, 2023.

Liu, Z., Cheng, M., Zhao, G., Yang, J., Liu, Q., and Chen, E. Improving time series forecasting via instance-aware post-hoc revision, 2025b.

Liu, Z., Yang, Z., Lin, X., Qiu, R., Wei, T., Zhu, Y., Hamann, H., He, J., and Tong, H. Breaking silos: Adaptive model fusion unlocks better time series forecasting, 2025c.

Luo, D. and Wang, X. Moderntcn: A modern pure convolution structure for general time series analysis. In *The twelfth international conference on learning representations*, pp. 1–43, 2024.

Nie, Y., Nguyen, N. H., Sinthong, P., and Kalagnanam, J. A time series is worth 64 words: Long-term forecasting with transformers. In *11th International Conference on Learning Representations, ICLR 2023*, 2023.

Ning, K., Pan, Z., Liu, Y., Jiang, Y., Zhang, J. Y., Rasul, K., Schneider, A., Ma, L., Nevmyvaka, Y., and Song, D. Ts-rag: Retrieval-augmented generation based time series foundation models are stronger zero-shot forecaster, 2025.

Oreshkin, B. N., Carpov, D., Chapados, N., and Bengio, Y. N-beats: Neural basis expansion analysis for interpretable time series forecasting, 2020.

Qiu, X., Hu, J., Zhou, L., Wu, X., Du, J., Zhang, B., Guo, C., Zhou, A., Jensen, C. S., Sheng, Z., and Yang, B. Tfb: Towards comprehensive and fair benchmarking of time series forecasting methods. *Proceedings of the VLDB Endowment*, pp. 2363–2377, 2024.

Qiu, X., Cheng, H., Wu, X., Hu, J., Guo, C., and Yang, B. A comprehensive survey of deep learning for multivariate time series forecasting: A channel strategy perspective, 2025a.

Qiu, X., Wu, X., Cheng, H., Liu, X., Guo, C., Hu, J., and Yang, B. Dbloss: Decomposition-based loss function for time series forecasting, 2025b.

Shao, Z., Wang, F., Xu, Y., Wei, W., Yu, C., Zhang, Z., Yao, D., Sun, T., Jin, G., Cao, X., Cong, G., Jensen, C. S., and Cheng, X. Exploring progress in multivariate time series forecasting: Comprehensive benchmarking and heterogeneity analysis. *IEEE Transactions on Knowledge and Data Engineering*, pp. 291–305, 2025.

Shi, X., Wang, S., Nie, Y., Li, D., Ye, Z., Wen, Q., and Jin, M. Time-moe: Billion-scale time series foundation models with mixture of experts, 2025.

Sun, Y., Xie, Z., Chen, D., Eldele, E., and Hu, Q. Hierarchical classification auxiliary network for time series forecasting, 2024.

Tang, P. and Zhang, W. Unlocking the power of patch: Patch-based mlp for long-term time series forecasting, 2024.

Tran, L., Nguyen, M., and Shahabi, C. Representation learning for early sepsis prediction. In *2019 Computing in Cardiology (CinC)*, pp. 1–4. IEEE, 2019.

Wang, H., Peng, J., Huang, F., Wang, J., Chen, J., and Xiao, Y. Micn: Multi-scale local and global context modeling for long-term series forecasting. In *11th International Conference on Learning Representations, ICLR 2023*, 2023.

Wang, H., Pan, L., Chen, Z., Yang, D., Zhang, S., Yang, Y., Liu, X., Li, H., and Tao, D. Fredf: Learning to forecast in the frequency domain, 2025a.

Wang, S., Wu, H., Shi, X., Hu, T., Luo, H., Ma, L., Zhang, J. Y., and Zhou, J. Timemixer: Decomposable multiscale mixing for time series forecasting, 2024a.

Wang, S., Li, J., Shi, X., Ye, Z., Mo, B., Lin, W., Ju, S., Chu, Z., and Jin, M. Timemixer++: A general time series pattern machine for universal predictive analysis, 2025b.

Wang, Y., Wu, H., Dong, J., Liu, Y., Long, M., and Wang, J. Deep time series models: A comprehensive survey and benchmark, 2024b.

Wang, Y., Wu, H., Dong, J., Qin, G., Zhang, H., Liu, Y., Qiu, Y., Wang, J., and Long, M. Timexer: Empowering transformers for time series forecasting with exogenous variables, 2024c.

Wei, K., Li, T., Huang, F., Chen, J., and He, Z. Cancer classification with data augmentation based on generative adversarial networks. *Frontiers of Computer Science*, 16(2):162601, 2022.

Woo, G., Liu, C., Kumar, A., Xiong, C., Savarese, S., and Sahoo, D. Unified training of universal time series forecasting transformers. In *ICML'24: Proceedings of the 41st International Conference on Machine Learning*, 2024.

Wu, H., Xu, J., Wang, J., and Long, M. Autoformer: Decomposition transformers with auto-correlation for long-term series forecasting. *Advances in neural information processing systems*, 34:22419–22430, 2021.

Wu, H., Hu, T., Liu, Y., Zhou, H., Wang, J., and Long, M. Timesnet: Temporal 2d-variation modeling for general time series analysis. In *11th International Conference on Learning Representations, ICLR 2023*, 2023a.

Wu, H., Zhou, H., Long, M., and Wang, J. Interpretable weather forecasting for worldwide stations with a unified deep model. *Nature Machine Intelligence*, pp. 602–611, 2023b.

Yang, H., Tang, J., Li, Z., and Lan, L. Dmsc: Dynamic multi-scale coordination framework for time series forecasting, 2025.

Yi, K., Zhang, Q., Fan, W., Wang, S., Wang, P., He, H., An, N., Lian, D., Cao, L., and Niu, Z. Frequency-domain mlps are more effective learners in time series forecasting. *Advances in Neural Information Processing Systems*, 36: 76656–76679, 2023.

Yu, X., Chen, Z., Ling, Y., Dong, S., Liu, Z., and Lu, Y. Temporal data meets lilm – explainable financial time series forecasting, 2023.

Zeng, A., Chen, M., Zhang, L., and Xu, Q. Are transformers effective for time series forecasting? In *Proceedings of the AAAI conference on artificial intelligence*, volume 37, pp. 11121–11128, 2023.

Zhou, H., Zhang, S., Peng, J., Zhang, S., Li, J., Xiong, H., and Zhang, W. Informer: Beyond efficient transformer for long sequence time-series forecasting. In *Proceedings of the AAAI conference on artificial intelligence*, volume 35, pp. 11106–11115, 2021.

A. Datasets

We conduct long-term forecasting experiments on 6 real-world datasets, including (1) ETT (ETTh1, ETTh2, ETTm1, ETTm2) contains 7 features of electricity transformer data from July 2016 to July 2018, which sampled at hourly (ETTh1, ETTh2) and 15-minute (ETTm1, ETTm2) intervals. (2) Electricity (ECL) records hourly electricity consumption data of 321 clients from 2012 to 2014. (3) Exchange collects the daily exchange-rate data from eight different countries. (4) Solar-Energy contains the solar power production of 137 PV plants in 2006, which is sampled every 10 minutes. (5) Weather includes 21 meteorological factors collected every 10 minutes from the Max Planck Biogeochemistry Institute's Weather Station in 2020. (6) Traffic contains hourly road occupancy rates from 862 sensors on San Francisco freeways. Meanwhile, we conduct short-term forecasting experiments on PEMS (PEMS03, PEMS04, PEMS07, PEMS08), which contains the public traffic network data in California with a 5-minute interval. The details of datasets are listed in Table 7.

Table 7. Dataset Descriptions. Num is the number of variable. Dataset size is organized in (Train, Validation, Test).

Name	Domain	Length	Num	Prediction Length	Dataset Size	Freq. (m)
ETTh1	Temperature	14400	7	{96,192,336,720}	(8545,2881,2881)	60
ETTh2	Temperature	14400	7	{96,192,336,720}	(8545,2881,2881)	60
ETTm1	Temperature	57600	7	{96,192,336,720}	(34465,11521,11521)	15
ETTm2	Temperature	57600	7	{96,192,336,720}	(34465,11521,11521)	15
Electricity	Electricity	26304	321	{96,192,336,720}	(18317,2633,5261)	60
Exchange	Exchange Rate	7588	8	{96,192,336,720}	(5120,665,1422)	1440
Traffic	Road Occupancy	17544	862	{96,192,336,720}	(12185,1757,3509)	60
Weather	Weather	52696	21	{96,192,336,720}	(36792,5271,10540)	10
Solar-Energy	Energy	52179	137	{96,192,336,720}	(36601,5161,10417)	10
PEMS03	Traffic Flow	26208	358	{12,24,48,96}	(15617,5135,5135)	5
PEMS04	Traffic Flow	16992	307	{12,24,48,96}	(10172,3375,3375)	5
PEMS07	Traffic Flow	28224	883	{12,24,48,96}	(16711,5622,5622)	5
PEMS08	Traffic Flow	17856	170	{12,24,48,96}	(10690,3548,3548)	5

B. Metrics Details

To evaluate forecasting performance for TSF, we utilize the mean square error (MSE) and mean absolute error (MAE). The calculations of metrics are as follows:

$$\text{MSE} = \frac{1}{n} \sum_{i=1}^n (\mathbf{Y}_i - \hat{\mathbf{Y}}_i)^2, \quad \text{MAE} = \frac{1}{n} \sum_{i=1}^n |\mathbf{Y}_i - \hat{\mathbf{Y}}_i|. \quad (17)$$

C. Hyperparameter Sensitivity

C.1. Size of Prototype Banks

The sizes of the Common Pattern Bank \mathcal{B}_c and Rare Pattern Bank \mathcal{B}_r determine the representational capacity and specialization degree of our Dual-Prototype Bank. To analyze their impact, we set $\mathcal{B}_c \in \{32, 64, 128, 256\}$ and $\mathcal{B}_r \in \{8, 12, 24, 32\}$ respectively on Weather and ETTh2 dataset. As shown in Figure 5, the results remains stable across a broad range of sizes, indicating that DPAD is not highly sensitive to the size of prototype banks. Extremely small banks may limit the ability to capture pattern diversity, while very large banks offer no further gain and may slightly degrade performance due to increased optimization difficulty. The above observation confirm that DPAD is robust across various cases without requiring delicate tuning.

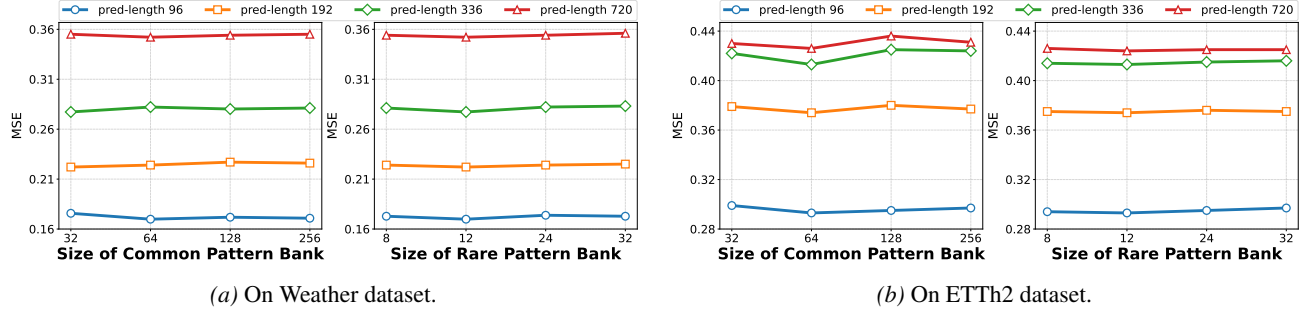


Figure 5. Hyperparameter sensitivity analysis with varying sizes of prototype banks on Weather dataset. Here we use iTransformer as backbone. Left is of common pattern set, right is of rare patterns set. The look-back length is fixed to 96.

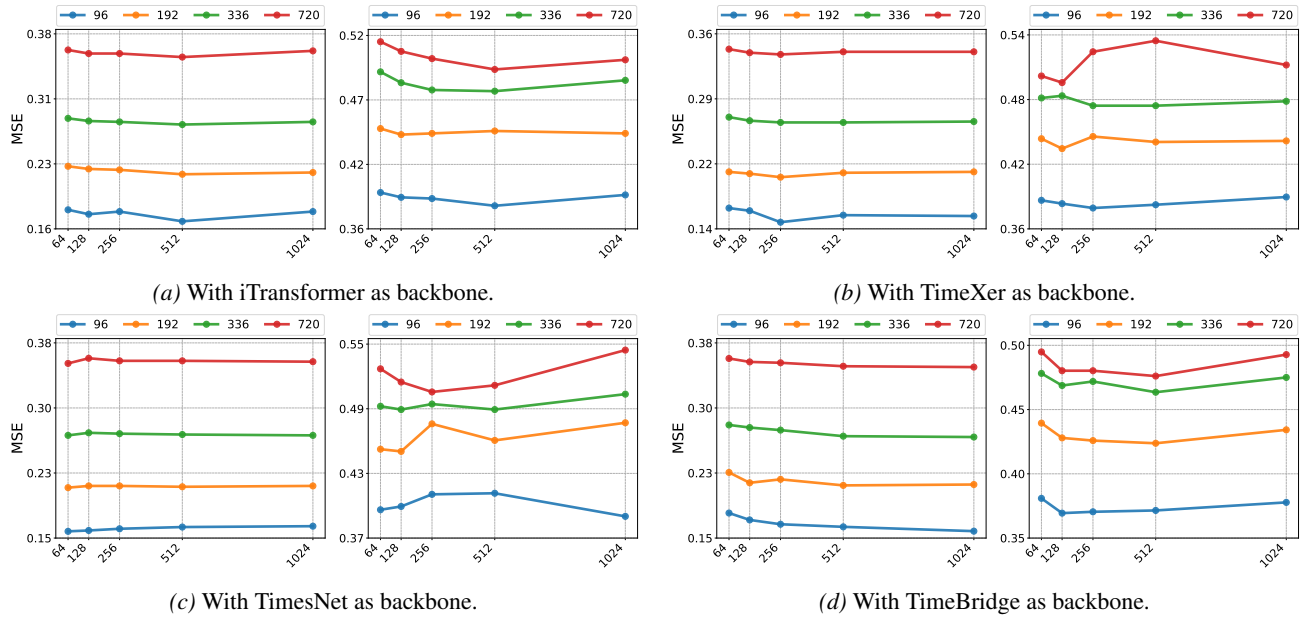


Figure 6. Hyperparameter sensitivity analysis on embedding dimension. For each backbone, forecasting results is on the Weather (left) and ETTh1 (right) datasets. The look-back length length is fixed to 96.

C.2. Embedding Dimension

The embedding dimension determines the richness of feature representations in the unified projection space. We vary $d_{\text{model}} \in \{64, 128, 256, 512, 1024\}$ on Weather and ETTh1 dataset with four backbone models to evaluate its impact. As shown in Figure 6, in most cases DPAD exhibits low sensitivity to the choice of embedding dimension. Performance does not degrade significantly even at relatively small dimensions, while larger dimensions provide only marginal gains. So we choose the optimal dimension at 128/256 in most cases. The above observation indicates that our dual-prototype architecture and routing mechanism are effective at capturing and utilizing pattern information without requiring a high dimension latent space. This property further simplifies the deployment of DPAD as a plug-and-play module.

C.3. Weights of DGLoss

The weight λ_{sep} , λ_{rare} , λ_{div} of the DGLoss control the strength of separation, rarity preservation, and diversity of temporal prototypes. To analyze their individual effects, we vary them in 0.001 – 2.0 on electricity and weather datasets. As shown in Figure 7,

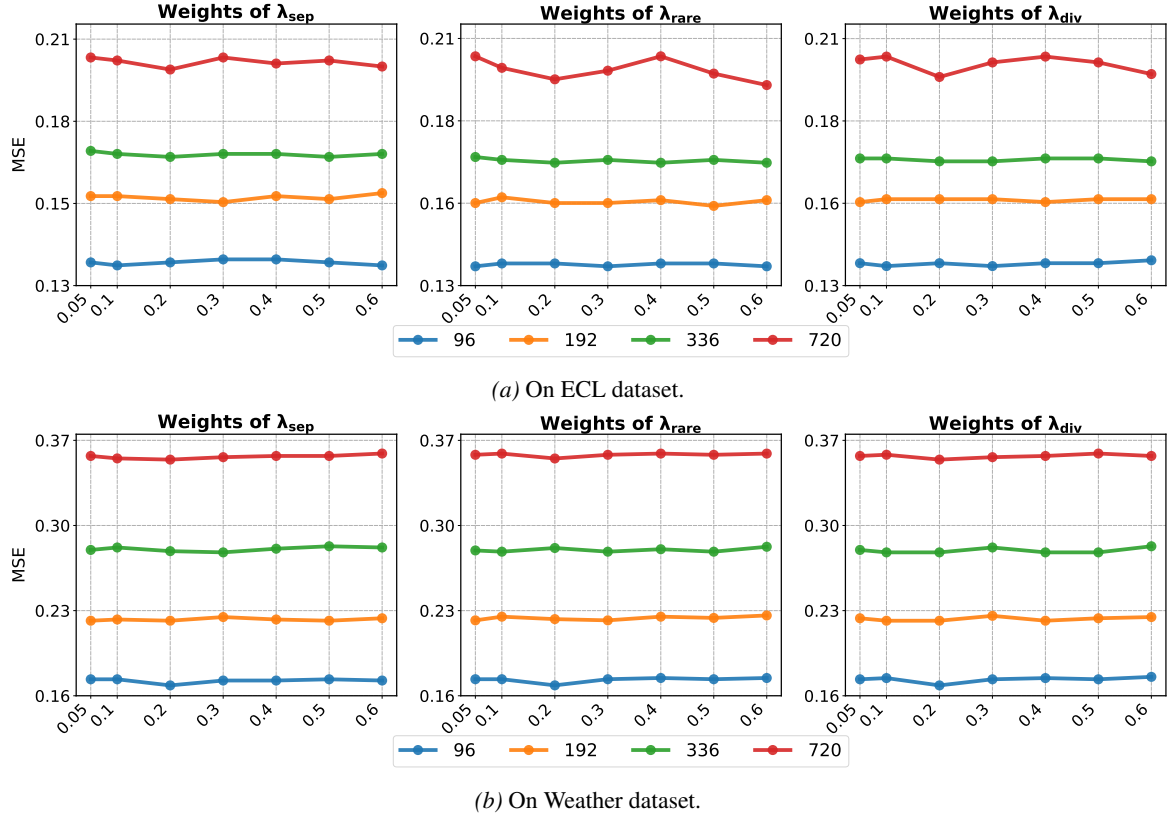


Figure 7. Hyperparameter sensitivity analysis on weights of DGLoss. Forecasting results is on the ECL and Weather datasets, and we use TimeBridge as backbone model. The look-back length length is fixed to 96.

D. Forecasting Visualization

To provide an intuitive and comprehensive view of the improvements brought by our DPAD framework, we present forecasting visualizations comparing the predictions of backbone models with and without DPAD across four representative datasets. As shown in Figure 8, the predictions with DPAD are closer to the ground truth. These visualization results serve as qualitative evidence that DPAD enables more flexible, context-aware, and accurate forecasting across diverse model architectures and temporal patterns.

E. Full Results

E.1. Main experiments

we evaluate DPAD on seven real-world TSF benchmarks spanning diverse domains. Table 8 shows the full results of long-term forecasting tasks on ETT (ETTh1, ETTh2, ETTm1, ETTm2), Electricity, Exchange, Solar, Weather, and Traffic datasets. Table 9 contains the full results of short-term forecasting tasks on PEMS (PEMS03, PEMS04, PEMS05, PEMS06) datasets. From full results, we can see that DPAD achieves consistent improvements on most backbones and datasets.

E.2. Ablation Results

Table 10 shows the full results of ablation studies discussed in the main text. From full results, we can see that each component in our DPAD framework plays an indispensable role.

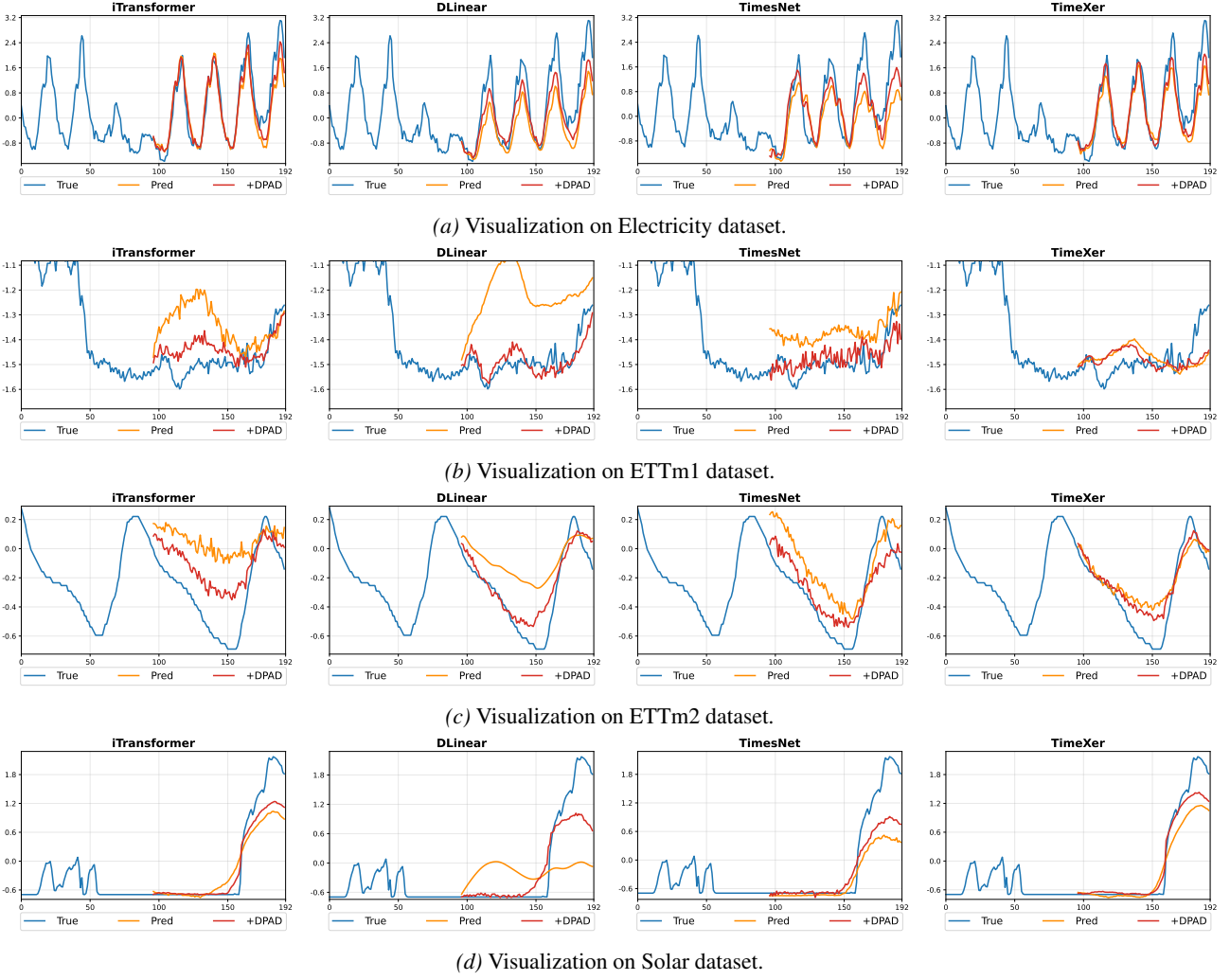


Figure 8. Forecasting visualization for backbone models with and without DPAD.

Table 8. Full results of long-term forecasting. All the results are selected from 4 different prediction lengths $\{96, 192, 336, 720\}$, and the look-back length is fixed to 96 for all baselines. The better results are highlighted in **bold**.

Methods	iTransformer				DLinear				TimesNet				TimeXer				TimeBridge				
	Ori		+DPAD		Ori		+DPAD		Ori		+DPAD		Ori		+DPAD		Ori		+DPAD		
Metric	MSE	MAE	MSE	MAE	MSE	MAE															
ETTh1	96	0.387	0.405	0.383	0.401	0.397	0.412	0.388	0.403	0.415	0.429	0.419	0.423	0.386	0.404	0.379	0.398	0.377	0.395	0.371	0.388
	192	0.441	0.436	0.433	0.423	0.446	0.441	0.431	0.432	0.479	0.466	0.471	0.460	0.429	0.435	0.433	0.430	0.427	0.425	0.423	0.421
	336	0.494	0.463	0.478	0.452	0.489	0.467	0.478	0.459	0.517	0.482	0.504	0.473	0.484	0.457	0.472	0.446	0.477	0.456	0.461	0.441
	720	0.488	0.483	0.492	0.482	0.513	0.511	0.501	0.506	0.505	0.490	0.512	0.496	0.544	0.513	0.483	0.493	0.521	0.498	0.473	0.474
	Avg	0.452	0.446	0.446	0.439	0.461	0.457	0.449	0.450	0.479	0.466	0.476	0.463	0.460	0.452	0.442	0.441	0.450	0.443	0.432	0.431
ETTh2	96	0.301	0.350	0.293	0.345	0.341	0.394	0.332	0.381	0.316	0.358	0.309	0.358	0.284	0.337	0.276	0.331	0.294	0.345	0.287	0.333
	192	0.380	0.399	0.374	0.393	0.482	0.479	0.466	0.471	0.415	0.414	0.397	0.407	0.366	0.391	0.366	0.392	0.377	0.395	0.359	0.380
	336	0.423	0.431	0.416	0.425	0.591	0.541	0.535	0.512	0.452	0.448	0.433	0.436	0.438	0.424	0.429	0.424	0.433	0.408	0.418	
	720	0.431	0.447	0.422	0.435	0.839	0.661	0.785	0.638	0.461	0.463	0.448	0.455	0.407	0.449	0.411	0.432	0.423	0.442	0.417	0.435
	Avg	0.383	0.406	0.376	0.399	0.563	0.518	0.529	0.500	0.411	0.420	0.396	0.414	0.373	0.403	0.369	0.396	0.379	0.403	0.367	0.391
ETTm1	96	0.341	0.376	0.332	0.369	0.346	0.374	0.334	0.369	0.336	0.375	0.329	0.371	0.318	0.356	0.320	0.358	0.324	0.362	0.311	0.345
	192	0.382	0.396	0.377	0.389	0.382	0.391	0.375	0.392	0.377	0.395	0.376	0.393	0.373	0.389	0.366	0.383	0.365	0.384	0.361	0.375
	336	0.420	0.421	0.411	0.412	0.415	0.415	0.405	0.415	0.418	0.420	0.405	0.409	0.412	0.387	0.407	0.394	0.407	0.392	0.397	
	720	0.487	0.456	0.484	0.451	0.473	0.451	0.465	0.443	0.541	0.481	0.493	0.464	0.460	0.450	0.451	0.441	0.462	0.444	0.455	0.431
	Avg	0.407	0.412	0.401	0.405	0.404	0.407	0.394	0.404	0.418	0.417	0.400	0.409	0.390	0.395	0.386	0.394	0.387	0.399	0.379	0.387
ETTm2	96	0.186	0.272	0.179	0.263	0.193	0.293	0.190	0.295	0.188	0.268	0.181	0.264	0.172	0.254	0.165	0.251	0.177	0.260	0.176	0.254
	192	0.252	0.312	0.245	0.306	0.284	0.361	0.273	0.353	0.250	0.306	0.243	0.304	0.241	0.302	0.238	0.300	0.243	0.303	0.242	0.298
	336	0.315	0.351	0.309	0.344	0.382	0.429	0.367	0.415	0.306	0.341	0.298	0.337	0.301	0.340	0.397	0.331	0.303	0.342	0.304	0.338
	720	0.415	0.408	0.409	0.405	0.558	0.525	0.508	0.501	0.420	0.405	0.402	0.398	0.394	0.395	0.396	0.393	0.401	0.399	0.409	0.397
	Avg	0.292	0.335	0.285	0.329	0.354	0.402	0.334	0.391	0.291	0.330	0.281	0.325	0.277	0.322	0.299	0.318	0.281	0.326	0.282	0.321
Electricity	96	0.148	0.241	0.147	0.234	0.211	0.302	0.202	0.293	0.163	0.267	0.159	0.269	0.241	0.244	0.141	0.241	0.143	0.239	0.135	0.228
	192	0.167	0.248	0.162	0.251	0.211	0.305	0.203	0.293	0.184	0.284	0.178	0.281	0.153	0.257	0.161	0.256	0.154	0.247		
	336	0.179	0.271	0.172	0.271	0.223	0.319	0.210	0.304	0.196	0.297	0.205	0.303	0.177	0.276	0.177	0.271	0.176	0.272	0.172	0.264
	720	0.208	0.298	0.201	0.289	0.258	0.351	0.243	0.332	0.232	0.325	0.243	0.331	0.229	0.321	0.210	0.306	0.204	0.297	0.201	0.288
	Avg	0.175	0.264	0.170	0.261	0.225	0.319	0.214	0.305	0.193	0.293	0.196	0.296	0.201	0.275	0.170	0.268	0.171	0.266	0.165	0.256
Exchange	96	0.088	0.208	0.081	0.202	0.098	0.233	0.095	0.228	0.115	0.242	0.097	0.224	0.094	0.214	0.086	0.205	0.113	0.236	0.084	0.201
	192	0.180	0.303	0.175	0.299	0.186	0.325	0.182	0.319	0.216	0.333	0.186	0.310	0.182	0.303	0.179	0.301	0.200	0.327	0.177	0.297
	336	0.331	0.418	0.326	0.414	0.325	0.434	0.329	0.442	0.375	0.444	0.360	0.434	0.384	0.448	0.350	0.426	0.364	0.440	0.339	0.421
	720	0.848	0.695	0.835	0.692	0.746	0.663	0.772	0.678	0.101	0.765	0.893	0.720	0.932	0.724	0.887	0.706	0.992	0.760	0.847	0.691
	Avg	0.361	0.406	0.354	0.401	0.338	0.413	0.345	0.417	0.201	0.446	0.384	0.422	0.398	0.422	0.375	0.409	0.417	0.440	0.361	0.402
Solar	96	0.207	0.237	0.199	0.221	0.290	0.378	0.240	0.299	0.223	0.256	0.211	0.249	0.198	0.244	0.191	0.235	0.204	0.245	0.196	0.212
	192	0.242	0.264	0.237	0.254	0.320	0.398	0.263	0.312	0.262	0.272	0.241	0.267	0.226	0.270	0.221	0.262	0.237	0.269	0.228	0.236
	336	0.251	0.277	0.249	0.273	0.353	0.415	0.279	0.314	0.287	0.299	0.257	0.291	0.239	0.281	0.231	0.275	0.251	0.283	0.247	0.256
	720	0.251	0.278	0.250	0.276	0.357	0.413	0.276	0.310	0.298	0.318	0.267	0.298	0.242	0.282	0.238	0.277	0.253	0.284	0.255	0.260
	Avg	0.237	0.264	0.233	0.256	0.330	0.401	0.264	0.308	0.267	0.286	0.244	0.276	0.226	0.269	0.220	0.262	0.236	0.270	0.231	0.241
Traffic	96	0.393	0.269	0.392	0.268	0.712	0.438	0.647	0.402	0.593	0.317	0.471	0.295	0.428	0.271	0.415	0.263	0.375	0.270	0.371	0.243
	192	0.412	0.277	0.407	0.271	0.662	0.417	0.599	0.380	0.618	0.327	0.493	0.309	0.447	0.280	0.442	0.273	1.411	0.803	0.397	0.254
	336	0.424	0.283	0.417	0.279	0.669	0.419	0.590	0.374	0.642	0.341	0.514	0.320	0.472	0.289	0.473	0.290	1.427	0.806	0.408	0.261
	720	0.459	0.301	0.447	0.293	0.709	0.437	0.616	0.385	0.679	0.350	0.517	0.307	0.522	0.310	0.435</					

Table 9. Full results of short-term forecasting. All the results are selected from 4 different prediction lengths $\{12, 24, 48, 96\}$, and the look-back length is fixed to 96 for all baselines. The better results are highlighted in **bold**.

Methods	iTransformer				DLinear				TimesNet				TimeXer				TimeBridge				
	Ori		+DPAD		Ori		+DPAD		Ori		+DPAD		Ori		+DPAD		Ori		+DPAD		
Metric	MSE	MAE	MSE	MAE	MSE	MAE	MSE	MAE	MSE	MAE	MSE	MAE	MSE	MAE	MSE	MAE	MSE	MAE	MSE	MAE	
PEMS03	12	0.069	0.175	0.067	0.169	0.122	0.245	0.102	0.218	0.088	0.195	0.066	0.172	0.068	0.179	0.077	0.183	0.075	0.183	0.072	0.178
	24	0.099	0.210	0.102	0.213	0.202	0.320	0.141	0.257	0.118	0.224	0.091	0.198	0.089	0.204	0.091	0.211	0.105	0.219	0.102	0.212
	48	0.164	0.275	0.169	0.281	0.334	0.428	0.226	0.329	0.169	0.268	0.137	0.244	0.137	0.253	0.134	0.249	0.171	0.284	0.169	0.278
	96	0.711	0.651	0.417	0.472	0.459	0.517	0.319	0.403	0.239	0.330	0.206	0.303	0.427	0.483	0.236	0.349	0.262	0.365	0.277	0.370
	Avg	0.260	0.327	0.188	0.283	0.279	0.377	0.197	0.301	0.153	0.254	0.125	0.229	0.180	0.279	0.134	0.248	0.153	0.262	0.155	0.259
PEMS04	12	0.766	0.709	0.115	0.241	0.147	0.272	0.114	0.233	0.092	0.202	0.073	0.179	0.293	0.397	0.083	0.198	0.097	0.206	0.093	0.198
	24	0.799	0.728	0.157	0.280	0.225	0.340	0.157	0.275	0.111	0.224	0.088	0.198	0.308	0.409	0.105	0.229	0.133	0.243	0.134	0.240
	48	1.041	0.882	0.229	0.341	0.356	0.437	0.239	0.343	0.152	0.266	0.118	0.234	0.339	0.425	0.146	0.272	0.215	0.319	0.216	0.313
	96	1.045	0.886	0.293	0.388	0.453	0.505	0.312	0.401	0.197	0.308	0.167	0.279	0.367	0.441	0.219	0.343	0.329	0.412	0.324	0.407
	Avg	0.912	0.801	0.199	0.312	0.295	0.388	0.205	0.313	0.138	0.250	0.111	0.222	0.326	0.418	0.138	0.261	0.193	0.295	0.192	0.289
PEMS07	12	0.068	0.169	0.065	0.161	0.116	0.241	0.100	0.210	0.075	0.179	0.063	0.162	0.061	0.165	0.056	0.161	0.067	0.168	0.066	0.163
	24	0.087	0.190	0.081	0.187	0.209	0.327	0.149	0.261	0.083	0.198	0.080	0.183	0.071	0.177	0.067	0.171	0.095	0.200	0.096	0.196
	48	0.122	0.231	0.118	0.225	0.397	0.456	0.269	0.347	0.128	0.235	0.118	0.221	0.100	0.208	0.109	0.211	0.145	0.252	0.148	0.248
	96	0.159	0.267	0.152	0.258	0.592	0.552	0.374	0.422	0.150	0.253	0.162	0.261	0.120	0.221	0.124	0.225	0.206	0.310	0.211	0.312
	Avg	0.109	0.214	0.104	0.207	0.328	0.394	0.223	0.310	0.109	0.216	0.105	0.206	0.088	0.192	0.089	0.192	0.128	0.232	0.130	0.230
PEMS08	12	0.081	0.183	0.078	0.179	0.153	0.259	0.148	0.234	0.158	0.192	0.082	0.185	0.146	0.198	0.088	0.204	0.080	0.184	0.075	0.178
	24	0.118	0.222	0.113	0.219	0.238	0.357	0.192	0.277	0.112	0.219	0.108	0.212	0.171	0.221	0.125	0.241	0.112	0.217	0.110	0.213
	48	0.202	0.292	0.210	0.294	0.473	0.515	0.310	0.353	0.231	0.198	0.166	0.221	0.220	0.270	0.208	0.283	0.186	0.278	0.181	0.272
	96	0.395	0.415	0.294	0.326	0.748	0.646	0.441	0.429	0.291	0.338	0.287	0.324	0.285	0.303	0.296	0.321	0.296	0.344	0.292	0.340
	Avg	0.199	0.278	0.173	0.254	0.403	0.444	0.272	0.323	0.198	0.236	0.160	0.235	0.205	0.248	0.179	0.262	0.168	0.255	0.164	0.251

Table 10. Full results of ablation study. All the results are selected from 4 different prediction lengths $\{96, 192, 336, 720\}$, and the look-back length is fixed to 96 for all baselines. The better results are highlighted in **bold**.

Case	+DPAD		w/o DDP		w/o Common Bank		w/o Rare Bank		w/ Additive		w/ Mean		w/ \mathcal{L}_{DGL}		w/o \mathcal{L}_{sep}		w/o \mathcal{L}_{rare}		w/o \mathcal{L}_{div}		
Metric	MSE	MAE	MSE	MAE	MSE	MAE	MSE	MAE	MSE	MAE	MSE	MAE	MSE	MAE	MSE	MAE	MSE	MAE	MSE	MAE	
Electricity	96	0.147	0.234	0.148	0.241	0.152	0.243	0.155	0.244	0.153	0.242	0.149	0.245	0.151	0.240	0.153	0.242	0.154	0.239	0.151	0.240
	192	0.162	0.251	0.167	0.248	0.167	0.259	0.170	0.261	0.169	0.260	0.167	0.263	0.171	0.264	0.168	0.262	0.166	0.259	0.165	0.260
	336	0.172	0.271	0.179	0.271	0.178	0.271	0.181	0.273	0.182	0.272	0.181	0.275	0.183	0.275	0.180	0.273	0.182	0.275	0.184	0.277
	720	0.201	0.192	0.208	0.298	0.216	0.303	0.225	0.310	0.213	0.298	0.212	0.294	0.217	0.305	0.209	0.301	0.212	0.297	0.208	0.299
	Avg	0.170	0.237	0.175	0.264	0.178	0.269	0.183	0.272	0.179	0.268	0.177	0.269	0.181	0.271	0.178	0.269	0.179	0.268	0.177	0.269
Weather	96	0.17	0.208	0.176	0.216	0.175	0.214	0.175	0.215	0.178	0.216	0.173	0.212	0.177	0.216	0.173	0.212	0.175	0.216	0.172	0.212
	192	0.223	0.256	0.225	0.257	0.229	0.257	0.230	0.262	0.228	0.259	0.227	0.260	0.231	0.263	0.229	0.260	0.230	0.261	0.229	0.261
	336	0.279	0.295	0.281	0.299	0.283	0.300	0.285	0.302	0.283	0.299	0.282	0.301	0.286	0.302	0.284	0.300	0.283	0.303	0.282	0.301
	720	0.355	0.347	0.361	0.353	0.362	0.353	0.361	0.351	0.361	0.352	0.359	0.352	0.363	0.352	0.360	0.352	0.359	0.352	0.358	0.352
	Avg	0.256	0.276	0.260	0.281	0.262	0.282	0.263	0.282	0.262	0.282	0.260	0.281	0.264	0.283	0.262	0.281	0.262	0.283	0.261	0.282
Traffic	96	0.392	0.268	0.393	0.269	0.477	0.337	0.395	0.272	0.396	0.270	0.459	0.325	0.457	0.323	0.426	0.314	0.433	0.310	0.468	0.333
	192	0.407	0.271	0.412	0.277	0.414	0.277	0.413	0.277	0.412	0.276	0.413	0.279	0.418	0.282	0.478	0.333	0.415	0.280	0.412	0.277
	336	0.417	0.279	0.424	0.283	0.425	0.283	0.427	0.284	0.425	0.284	0.425	0.286	0.429	0.286	0.424	0.282	0.493	0.340	0.425	0.282
	720	0.447	0.293	0.459	0.301	0.531	0.359	0.457	0.300	0.454	0.299	0.457	0.301	0.459	0.302	0.529	0.357	0.461	0.301	0.458	0.303
	Avg	0.416	0.278	0.422	0.282	0.462	0.314	0.423	0.283	0.422	0.282	0.439	0.298	0.441	0.298	0.464	0.322	0.450	0.308	0.441	0.299
Solar	96	0.199	0.221	0.207	0.237	0.206	0.239	0.204	0.233	0.205	0.247	0.203	0.236	0.210	0.241	0.208	0.241	0.209	0.240	0.206	0.243
	192	0.237	0.254	0.242	0.264	0.2															